Measurements of Ocean Surface Stress Using Aircraft Scatterometers

DAVID E. WEISSMAN

Department of Engineering, Hofstra University, Hempstead, New York

FUK K. LI, SHU-HSIANG LOU, SON V. NGHIEM, AND GREGORY NEUMANN

Jet Propulsion Laboratory, California Institute of Technology, Pasadena, California

ROBERT E. MCINTOSH, STEVEN C. CARSON, AND JAMES R. CARSWELL

Department of Electrical Engineering, University of Massachusetts, Amherst, Massachusetts

HANS C. GRABER

Rosenstiel School of Marine and Atmospheric Sciences, University of Miami, Miami, Florida

ROBERT E. JENSEN

Coastal Engineering Research Center, U.S. Army Corps of Engineers, Vicksburg, Mississippi

(Manuscript received 23 January 1996, in final form 20 November 1996)

ABSTRACT

Scatterometer model functions that directly estimate friction velocity have been developed and are being tested with radar and in situ data acquired during the Surface Wave Dynamics Experiment (SWADE) of 1991. K_u-band and C-band scatterometers were operated simultaneously for extensive intervals for each of 10 days during SWADE. The model function developed previously from the FASINEX experiment converts the K_u-band normalized radar cross-section (NRCS) measurements into friction velocity estimates. These are compared to in situ estimates of surface wind stress and direction across a wide area both on and off the Gulf Stream (for hourly intervals), which were determined from buoy and meteorological measurements during February and March 1991. This involved the combination of a local, specially derived wind field, with an ocean wave model coupled through a sea-state-dependent drag coefficient. The K_u-band estimates u_* magnitude are in excellent agreement with the in situ values. The C-band scatterometer measurements were coincident with the K_u-band NRCSs, whose u_* estimates are then used to calibrate the C band. The results show the C-band NRCS dependence at 20°, 30°, 40°, and 50° to be less sensitive to friction velocity than the corresponding cases for K_u band. The goal is to develop the capability of making friction velocity estimates (and surface stress) from radar cross-sectional data acquired by satellite scatterometers.

1. Introduction

It has been about 20 years since the Seasat-A scatterometer first provided global surface wind estimates. These were based on algorithms calibrated with wind speed data and were intended to provide wind vectors, not stress estimates (Pierson 1990). In the interim, there have been numerous expressions from members of the remote sensing community calling for direct estimates of friction velocity and stress using algorithms specifically developed for this purpose (O'Brien 1982). Official publications of the NASA Scatterometer (NSCAT) (Freilich 1985) and the World Ocean Circulation Experiment (WOCE) (Freilich 1995) projects indicate that wind stress is one of the required measurements.

The long-term goal of this research is to provide direct estimates of global sea surface wind stress, derived from satellite scatterometer observations. These radar cross-section observations will be utilized by new, empirically derived model functions based on the relationship between normalized radar cross section (NRCS) and friction velocity at the surface.

The wind forcing, or wind stress is the turbulent vertical flux of horizontal momentum. This is equal to the integral of the momentum flowing into all the wave components (Komen 1994). The magnitude of the wind stress, in terms of the wind speed U, at a reference height is

Corresponding author address: Dr. David E. Weissman, Department of Engineering, Hofstra University, Hempstead, NY 11550-1090.
E-mail: eggdew@vaxc.hofstra.edu

$$\tau = \rho C_D U^2,$$

where ρ is the air density and C_D is the drag coefficient. The drag coefficient depends on atmospheric stratification, wave state, wave age, and atmospheric homogeneity (Geernaert 1990; Cavaleri et al. 1994; Janssen 1992). It contributes a large amount of uncertainty when using satellite-derived wind fields to estimate global sea surface stress. In terms of the friction velocity u_*, the stress is

$$\tau = \rho u_*^2.$$

The high-frequency portion of the sea surface spectrum, which has the most direct effect on the microwave backscatter and radar cross section, is usually perceived to be a direct function of u_* (Phillips 1988).

The current major missions of the NSCAT project and the European Remote Sensing Satellite (ERS) scatterometer project to develop global-scale wind estimates as their continuous data product are well organized and in progress. However, there has never been a comparable effort to develop and implement a similar model function for surface stress. Therefore, the usual practice in applications that require stress estimates is to convert the satellite wind estimates, coupled with a drag coefficient estimate, into a stress quantity. While it has been known for some time how the drag coefficient depends on speed (Smith 1988; Anderson 1993), numerous recent studies have also shown how important the influence of sea state, wave age, and mixed sea conditions are to the magnitude of the drag coefficient (Geernaert 1990; Nordeng 1991; Smith et al. 1992; Donelan et al. 1993). None of this knowledge can be utilized with a wind speed estimate because the satellite scatterometers do not have any means of independently obtaining coincident sea state, swell, or spectrum information that could be used to support an algorithm for a multivariable drag coefficient. Of course, a friction velocity model function can go to the heart of the matter, since the drag coefficient dependencies are built in during its creation.

The model functions (K_u band for NSCAT and C band for *ERS-1* and *ERS-2*) for friction velocity described below were derived from major large-scale field experiments, in which airborne scatterometers collected data over a wide range of oceanic and atmospheric conditions, while coincident in situ observations were also made. The results presented in this paper illustrate the performance and potential accuracy of these model functions using independent estimates of u_* for this evaluation. Significant progress was made with the Frontal Air–Sea Interaction Experiment (FASINEX) data analysis (Li et al. 1989; Weissman et al. 1994), which indicated a more direct physical relationship between the radar cross section and friction velocity, than with wind speed in many situations (at a particular reference height).

Part of the motivation for conducting airborne radar scatterometer field measurements during FASINEX and the Surface Wave Dynamics Experiment (SWADE) was to create a database for the development of a friction velocity algorithm. This effort began in the mid-1980s in response to O'Brien et al. (1982). It was vigorously noted then that, ''ocean surface wind stress measurements are needed to drive ocean circulation models.'' In the interim, no satisfactory techniques have been found that estimate the stress from radar cross-sectional measurements. There have been no other aircraft scatterometer flight programs that have gathered any meaningful stress measurements for empirical algorithm development, to the best of the authors' knowledge, beyond those mentioned here.

There are several examples in the literature of studies concerned with utilizing satellite wind estimates from *ERS-1* and/or NSCAT simulations. The simulations by Barnier et al. (1991) and (1994) depend on estimates of sea surface stress. The only recourse they have is to start with wind estimates and then assume a constant drag coefficient across wide expanses of the ocean. The study of the Indian Ocean and tropical Pacific using actual *ERS-1* wind estimates by Legler and O'Brien (1993) leaves some discrepancies between the predictions of their ocean model and sea level data. A recent study by Caruso et al. (1994a) used *ERS-1* wind forcing to study the California, North Equatorial, and Kuroshio Currents, with mixed results. An important common issue in all of these instances is how to distinguish between the differences caused by deficiencies of a particular ocean model and those resulting from having to use wind estimates from the satellite sensors, instead of direct the wind stress values.

2. Background

a. Normalized radar cross section and algorithms

Even though the fundamental basis of the microwave radar cross section of the sea surface is the reflection of the transmitted electromagnetic waves from the rough surface (Plant 1990), its association with the surface wind stress has been justified from both theoretical (Phillips 1988, the shortwave dependence on u_*) and experimental (empirical) viewpoints. Notwithstanding the multitude of physical variables that influence the surface roughness, the principal motive of ''scatterometry'' is to convert the NRCS into an estimate of the most likely value of either the wind magnitude and direction (Pierson 1990), or the friction velocity (and stress direction). It therefore follows that for purposes of wind vector scatterometry, the mathematical representation for the NRCS can be expressed as a function of the wind and radar parameters:

$$\sigma^0 = f(u_*, \phi, \theta, p),$$

where u_* is the magnitude of the friction velocity, ϕ is the *relative* azimuthal angle between the plane of incidence of the radar wave and the stress direction, θ is

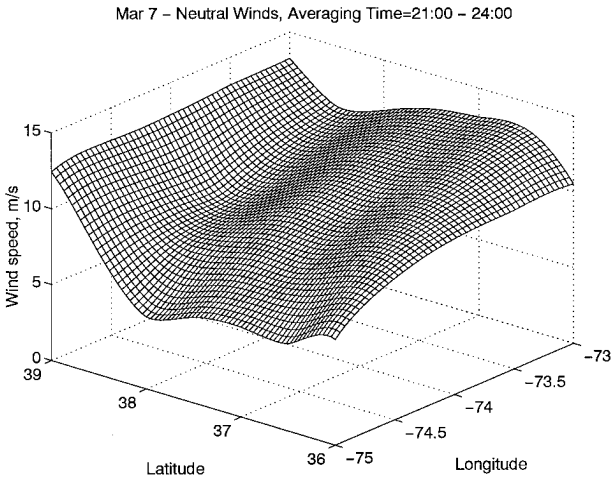

FIG. 1. Magnitude of the neutral stability wind speed estimated by Oceanweather, Inc.–University of Miami methods, in the region where the airborne scatterometers operated, and spanning the same time interval. This is an average of four hourly estimates, on 7 March. Resolution of 0.25° was interpolated to smaller grid.

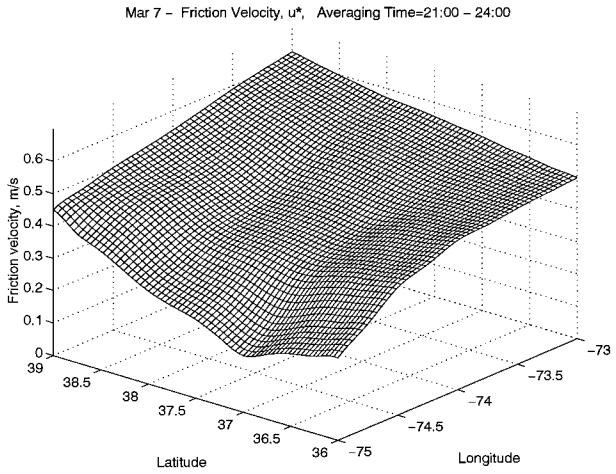

FIG. 3. Magnitude of the friction velocity estimated by Oceanweather, Inc.–University of Miami methods, in the region where the airborne scatterometers operated, and spanning the same time interval. This is an average of four hourly estimates, on 7 March. Resolution of 0.25° was interpolated to smaller grid.

the incidence angle (relative to nadir), and p represents the polarization, either H or V. Numerous studies involving satellite scatterometers (Wentz et al. 1984; Bentamy et al. 1994) have demonstrated that the azimuthal angle dependence can be separated from the incidence angle and friction velocity functions using the three-term Fourier series:

$$\sigma^0 = A_0(u_*, \theta) + A_1(u_*, \theta)\cos(\phi) + A_2(u_*, \theta)\cos(2\phi).$$

The specific functional dependence adopted for each of the empirical models for the A's varies substantially among different investigators and research groups. At a glance, we can see that the A_0 term equals the azimuthally averaged σ^0. This has some convenience in using it to estimate u_*, since there is no need to measure the wind or stress direction. This attribute was utilized in the studies to be presented in this paper. The A_1 term embodies the upwind–downwind difference. The following discussion will explain the recent history of the algorithm development for the A's in terms of u_*, and their application to the SWADE aircraft scatterometer studies.

b. FASINEX

FASINEX was a cooperative program to investigate the role of horizontal variability in air–sea interaction

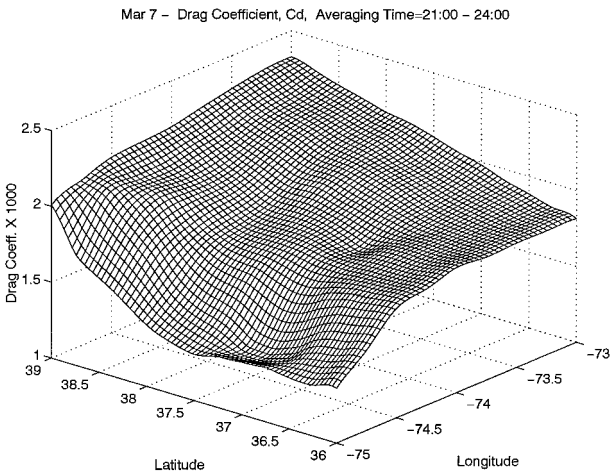

FIG. 2. Magnitude of the drag coefficient estimated by Oceanweather, Inc.–University of Miami methods, in the region where the airborne scatterometers operated, and spanning the same time interval. This is an average of four hourly estimates, on 7 March. Resolution of 0.25° was interpolated to smaller grid.

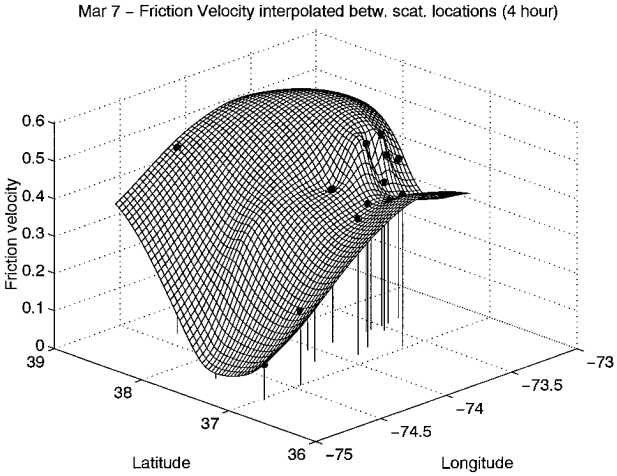

FIG. 4. Spatial variation of the friction velocity inferred from the K_u-band scatterometer measurements on 7 March, during a 4-h period. Each point is based on the average radar cross section over a 10–15-km flight segment. There are 19 data points used to create this mesh plot. Vertical lines indicate actual locations.

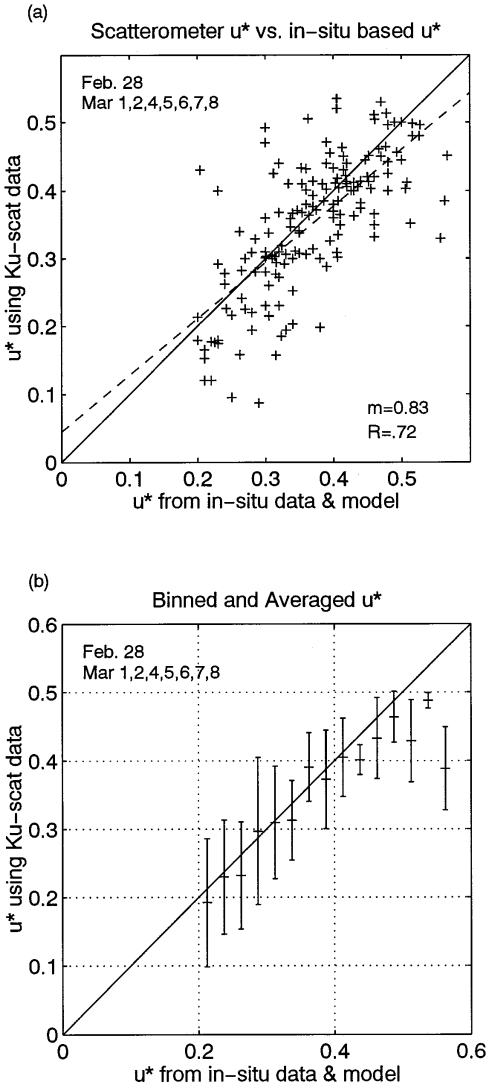

FIG. 5. Results from eight flight days; comparison from temporally and spatially coincident u_* estimates between scatterometer estimates (ordinate) versus those from in situ data using Oceanweather, Inc.–University of Miami analysis (abscissa). Solid line represents equality. (a) All individual points plotted (crosses); dashed line represents the regression line (m is slope of regression line and R is multiple correlation coefficient). (b) The range of the abscissa values was divided into bins of 0.025 m s^{-1} width. The mean of the ordinates of all points in each bin was plotted, with error bars representing the standard deviation.

in the vicinity of a sea surface temperature front. It took place during the winter/spring of 1985/86 (Stage and Weller 1985, 1986). There were coincident airborne scatterometer measurements of the ocean surface radar cross section at K_u band with wind speed and wind stress measured close to the surface, at both H and V polarizations.

The NASA–Jet Propulsion Laboratory K_u-band scatterometer data were obtained from 10 measurement flights during FASINEX. A total of approximately 30 h of data were collected under a wide range of sea and environmental conditions (Li et al. 1989). Winds encountered ranged from 2 to 20 m s^{-1}. Stress measurements were inferred from shipboard instruments and from aircraft flying at low altitudes, closely following the scatterometer.

These data have been analyzed to study separate, new model functions for both wind speed and surface friction velocity (square root of kinematic wind stress) and to better understand the physics of the air–sea interaction across a variety of spatial scales. These studies indicate that the surface stress has a more direct and consistent influence on the radar cross section than does the neutral wind speed (Weissman et al. 1994). In situations where the purpose of the scatterometer is to estimate surface wind stress, the use of the NRCS with a neutral stability wind algorithm and drag coefficient model to infer friction velocity does not produce results as close to the in situ measurement of friction velocity as does the FASINEX model. This case study for both H and V polarizations, for $0.15 < u_* < 0.7$ m s^{-1}, at incidence angles of 20°, 30°, 40°, and 50° can be seen in this reference.

c. SWADE

SWADE took place off the east coast of the United States in the region 35°–42°N and 70°–76°W during the period from October 1990 to March 1991. The objectives of SWADE include the direct measurement of wind stress and sensible and latent heat fluxes that, in conjunction with detailed measurements of the sea state, analyze the relationship between variability in the fluxes and sea state (Weller et al. 1991). It is precisely this variability in the momentum flux, related to the longwave sea state, that will affect the small scale roughness (which controls the microwave radar cross section) of the surface in a manner that can best be perceived with a friction velocity model function. Flight lines that crossed the western Gulf Stream boundary often observed strong gradients in the surface stress. This created interesting radar signatures.

The aircraft scatterometer measurements during SWADE took place between 27 February and 9 March 1991, during the third intensive observation period (IOP 3) of the entire project. The principal experiment area was east of the Virginia coast, in the vicinity of NOAA–NDBO, the Coastal Engineering Resource Center (CERC), and other buoys (near 37°N, 74°W) (Caruso et al. 1994a,b). The detailed experiment scenario and the descriptions of the radar instruments (and calibrations) can be found in Nghiem et al. (1995) and Carswell et al. (1994).

The K_u-band radar (NUSCAT, operating at 14 GHz) (Nghiem et al. 1995) and the C-band (C-SCAT, at approximately 5 GHz, V-pol) radar were mounted for simultaneous and collocated observations, on a NASA C-130B aircraft (McLaughlin et al. 1991; Carson 1992; Carswell et al. 1995). The NUSCAT antenna is a parabolic dish with a peak gain of 32 dB and a two-way

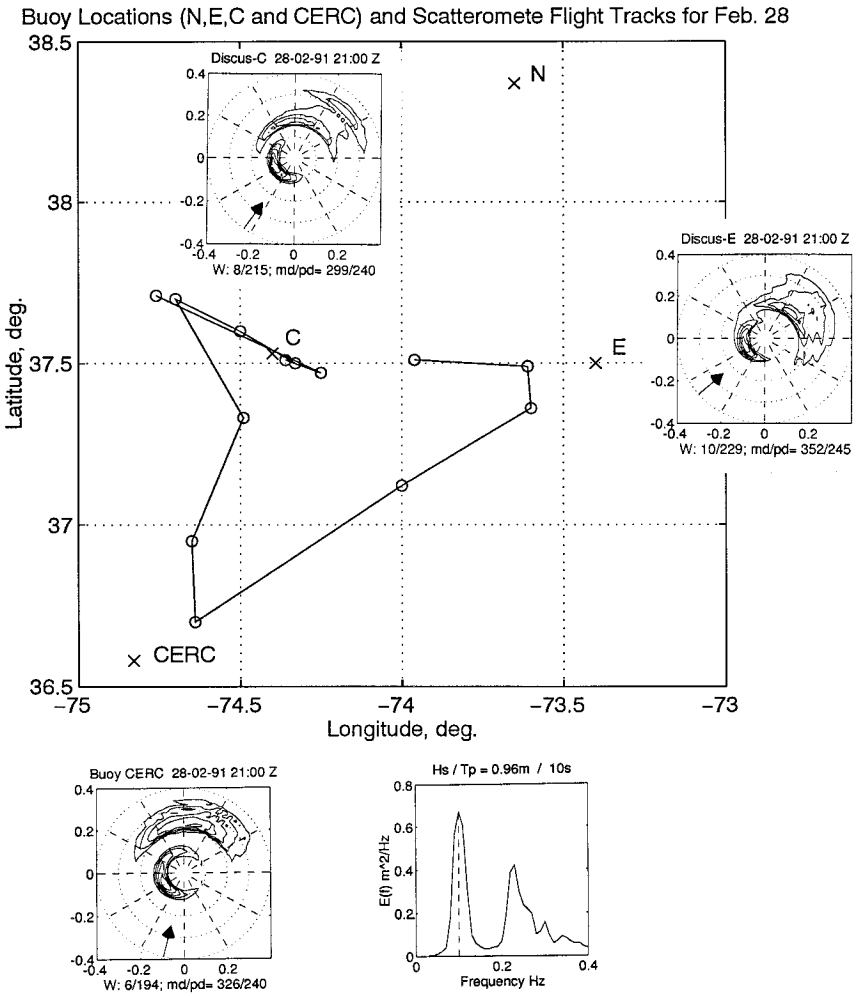

FIG. 6. A map indicating the principal flight tracks for the NASA C-130 aircraft and some buoy locations for the K_u-radar data collected on 28 February 1991. The buoy identifications are C, E, N, and CERC. The solid lines display the aircraft ground track, and coincident directional wave spectra are overlaid.

equivalent beamwidth of 4°. The transmitted peak power can be either 10 or 250 W, and a selection of H-pol or V-pol can be made for each azimuth scan sequence, at a fixed incidence angle. The latter were stepped to be among 20°, 30°, 40°, or 50°. The basic measurement of the NRCS is computed from a 0.5-s average of the returning echos. Both antennas rotated azimuthally in a nearly complete circle at each selected incidence angle. During flight segments where the aircraft follows a straight path, typically 50–100 km long, the usual scan interval for one cycle of antenna rotation lasts 2–3 min for each set of radar parameters. This corresponded to one revolution for the K_u-band antenna. During this cycle time the aircraft moves 14–20 km.

The C-SCAT radar operates only at V-pol, in the range from 4.98 to 5.7 GHz with a peak power of 2 W. The antenna two-way beamwidth is about 5°; the incidence angle is steered from 20° to 50° with frequency adjustment. The C-band antenna rotation rate is 20 rpm, resulting in multiple looks at each azimuth angle. Successive flight-line segments may be averaged together. The absolute accuracy of the surface radar sections measured by both of these instruments is estimated to be ± 1 db. It can be affected by several system component variables, with signal-to-noise ratio being of relatively less concern. Full details of instrument design and calibration can be found in Carswell et al. (1994).

d. Scatterometer-derived estimates of u_*

K_u-band and C-band scatterometers were operated simultaneously for extensive intervals for each of 10 days during SWADE. The model function that was developed previously from the FASINEX experiment converts the K_u-band NRCS measurements into friction velocity. The NUSCAT data were in a form such that A_0 could be easily calculated for each azimuth rotation. For the specific incidence angle and polarization of that scan, the

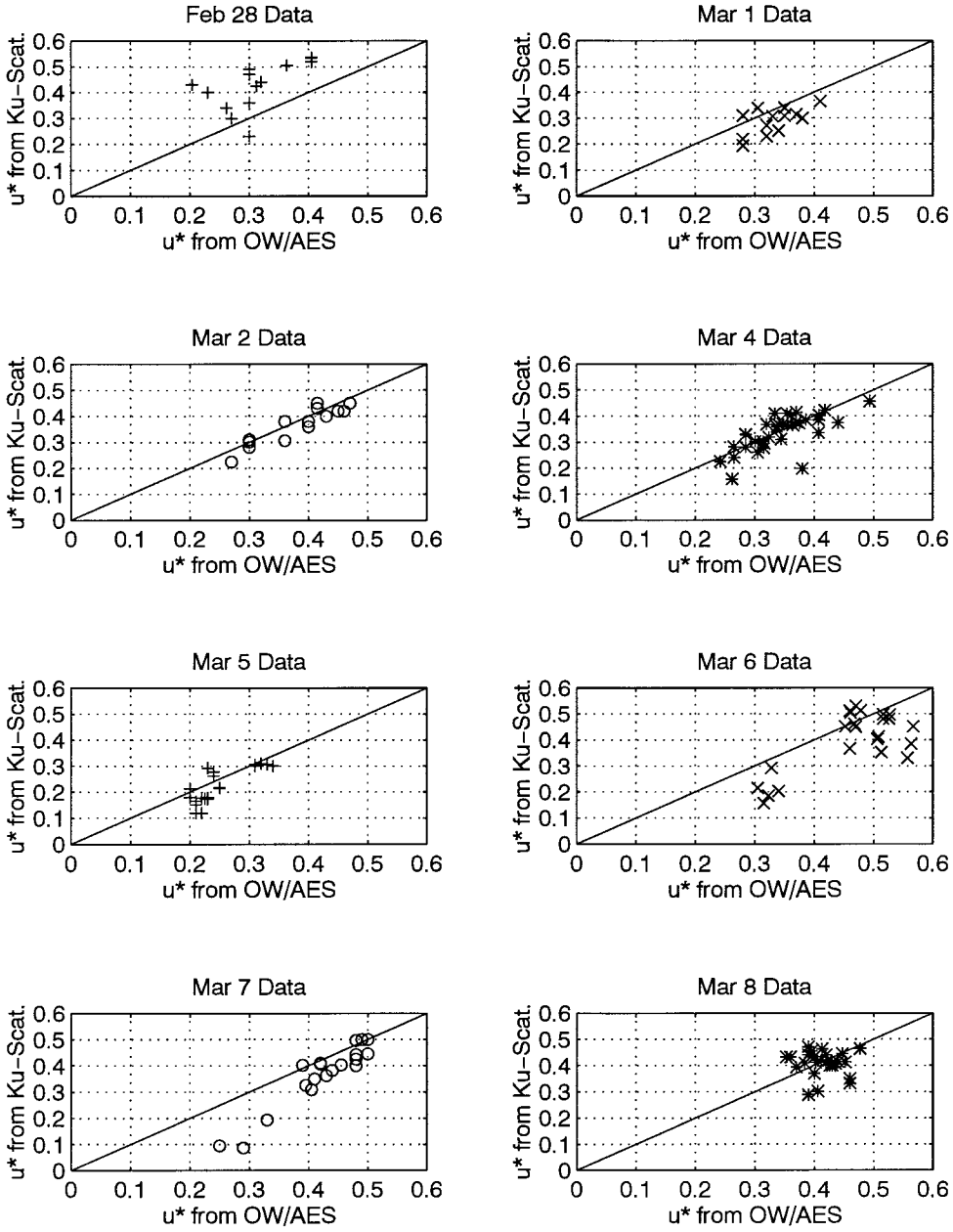

FIG. 7. Separate day presentations of the data in Fig. 5. The results are from eight flight days; comparison from temporally and spatially coincident u_* estimates between scatterometer estimates (ordinate) versus those from Oceanweather, Inc.–University of Miami (abscissa). Solid line represents equality. The quality of agreement between the two different methods can be observed for individual days.

value of A_0 is inverted into a u_* estimate using the matching FASINEX algorithm.

These u_* estimates could then be used to develop a C-band (5 GHz) algorithm for u_*. These estimates of friction velocity serve as the coincident surface measurements to calibrate the C-band system. The goal is to develop a model function for C band with the capability of making friction velocity estimates (and surface stress) from NRCS data acquired by the *ERS-1* satellite scatterometer.

The results to be presented will show the C-band NRCS dependence at 20°, 30°, 40°, and 50° to be less sensitive to friction velocity (smaller power-law exponents) than the corresponding cases for K_u band. This is to be expected, based on the laboratory measurements of Jahne and Riemer (1990), in which they were able to observe the u_* dependence of centimeter waves of different sizes, some of which closely matched our two Bragg waves for the K_u- and C-band scatterometers. The analysis of these radar data provides results that are

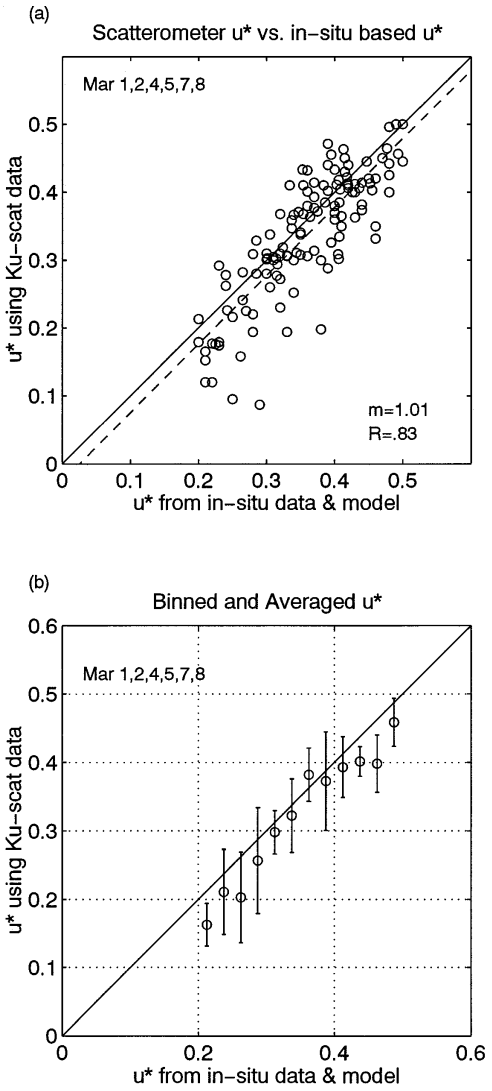

FIG. 8. Results from six flight days, with datasets from 28 February and 6 March omitted. Graphical format same as Fig. 5.

suitable for the development of a full algorithm for C-band (for all incidence and azimuthal angles) (Weissman 1994; Davidson et al. 1995).

Spatial variations of u_* across the Gulf Stream derived from the K_u-band radar data are studied in conjunction with supporting measurements of air–sea temperature, wind, and wave fields. These u_* estimates were then compared with the approximately coincident and concurrent friction velocity estimates derived from the SWADE wave hindcast model prediction of IOP 3 (Caruso et al. 1994b). These in situ estimates were updated every hour and spanned the entire SWADE region of interest. The SWADE buoys provide both physical oceanographic and meteorological data at points within the flight pattern. Wind conditions surveyed in this study ranged from 5 to 12 m s^{-1}. A detailed discussion of the analysis of the in situ measurements and related data appears in the following section. This comparison between the radar and in situ estimates of u_* serves as an independent test of the K_u-band FASINEX algorithm.

3. In situ measurements, analysis, and predictions

During this period of SWADE there were no *direct* measurements of u_* being made at the buoys. The bulk-derived values would not be sufficiently acceptable because the drag coefficient it used lacked sea state information. In any case, any direct data obtained from the buoys would be too restricted in spatial extent to be useful for this large area survey.

Six alternative wind fields were originally employed in the analysis of SWADE IOP 3 discussed in Caruso et al. (1994b). However, for this study we used the results from the wave simulation forced by the wind field of Oceanweather, Inc. (OWI). This wind field was derived by intensive manual kinematic reanalysis using all conventional and special SWADE meteorological data. Details of the wind field reanalysis procedures and methodologies are described in Cardone et al. (1995). The intent of the OWI analysis is to resolve the ''synoptic scale'' wind field at 3-h intervals on a grid spacing 0.5° in latitude and longitude covering the western North Atlantic or SWADE regional domain. The accuracy of the wind field was determined by comparing the measured winds in the SWADE array off the middle-Atlantic east coast with the model winds at the four closest grid points surrounding the buoy location. In the study of SWADE IOP 1, it was shown that the OWI wind fields provided sufficiently high spatial and temporal resolution to predict accurately the wave field during an intense mesoscale storm event (Graber et al. 1994; Cardone et al. 1995).

The ocean wave model used in the simulations described here is the third-generation wave model (WAM). A very detailed description of the physical framework of the WAM model and its numerous applications can be found in Komen et al. (1994). The version of the model implemented here is the cycle-4 release of WAM, or WAM-4, in which the atmospheric boundary layer is coupled to the wave model following Janssen (1991). In WAM-4, the evolution of the directional wave spectrum is specified on spherical coordinates defined by latitude and longitude, and is determined from the integration of the energy balance equation (e.g., Graber et al. 1995). Here we only consider deep water physics in the propagation and the source terms. The wave current option to include surface currents in this analysis was turned off. The three source terms consist of an empirically based wind input function, the nonlinear energy transfer resulting from resonant wave–wave interactions, and the dissipation due to wave breaking or the white-capping mechanism. Additional modifications of the source terms include a quadratic dependency of the wind input on the ratio of friction velocity to wave celerity and a dissipation that is proportional to the

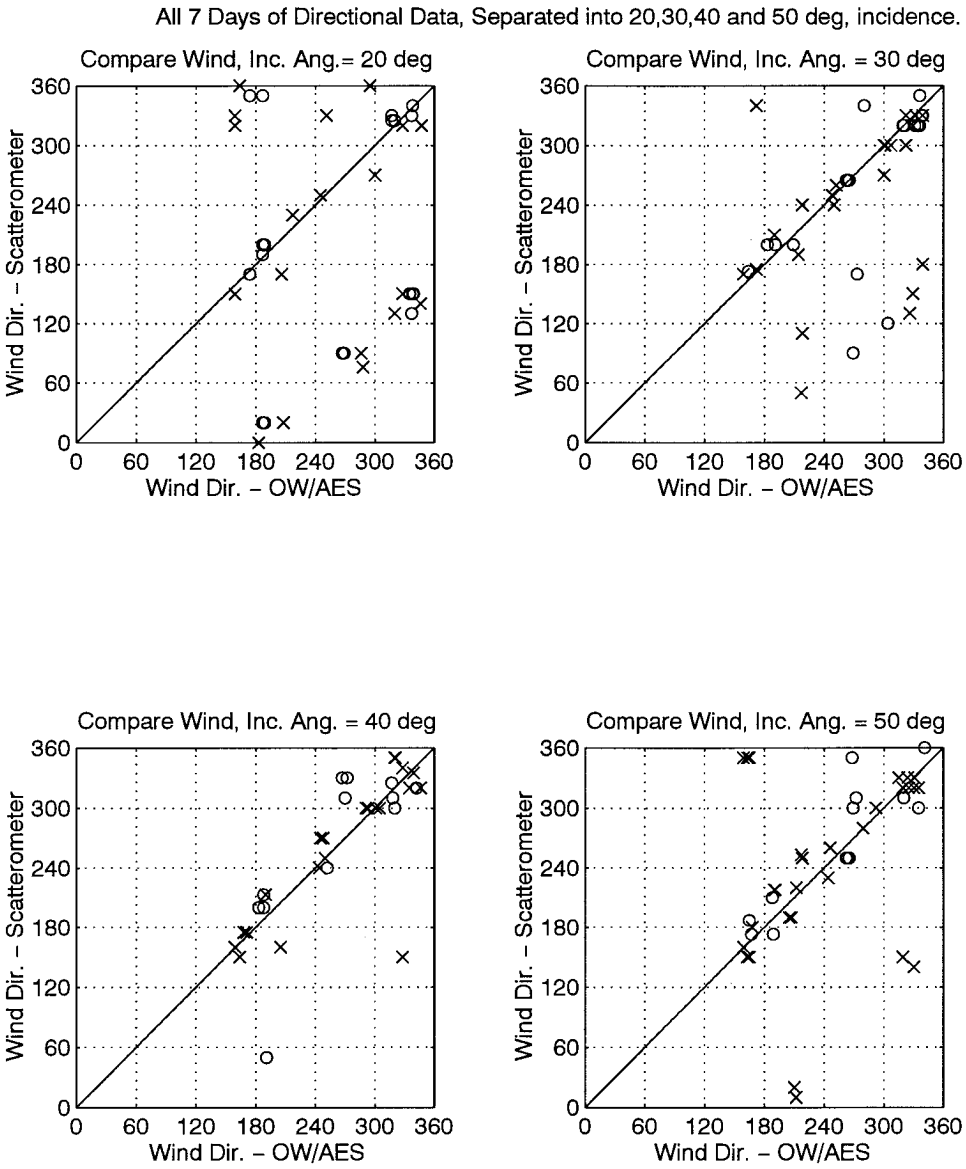

FIG. 9. Comparison between the estimates of the wind direction, separated by both incidence angle and polarization. Comparisons between scatterometer-derived wind direction (by selecting the direction of each azimuthal maximum) and estimates from Oceanweather, Inc.–University of Miami group. The V-pol data symbols are crosses; H-pol data are circles.

fourth power of the frequency. The wind input is given at standard height, usually 10 m, and the surface stress is calculated internally within the wave model as a function of both wind speed at height and stage of wave development (i.e., a sea-state-dependent drag coefficient).

WAM-4 was implemented on a nested grid system to represent the BASIN and regional SWADE domains. The basin grid covers the entire North and South Atlantic Oceans with a grid of 1° spacing. The basin grid hindcast with WAM-4 was run first and only once, using the European Centre for Medium-Range Weather Forecasts (ECMWF) 6-h wind fields as input. This simulation was started 5 days prior to, and continued throughout, the simulation period (25 February–9 March 1991) to provide overall spinup and continuous background wave conditions in the Atlantic Ocean and provide directional spectra along the ocean boundaries of the regional model. The regional model covers the western North Atlantic with a grid spacing of 0.25° latitude and longitude. Directional wave spectra are supplied from the basin grid to the eastern and southern boundaries to permit propagation of Southern Hemisphere swell into the SWADE region. The regional run was initially spun up with ECMWF winds over the 5 days prior to IOP 3 with input generated from the basin

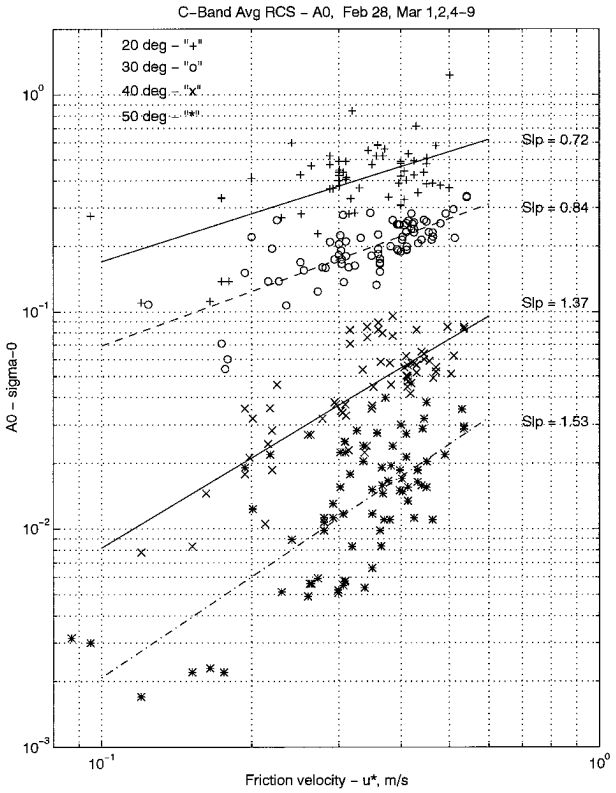

FIG. 10. The measured average C-band NRCS, A_0, at each incidence angle (A_0) versus u_*. Data spans nine flight days, duration of data collection at each incidence angle is 1–5 min. The magnitude of u_* is estimated from the simultaneous measurement of A_0 from the K_u-band radar cross sections.

run. For the simulation period of IOP 3, we then used the OWI wind fields to predict the directional wave field and its parameters as well as the sea-state-dependent drag coefficient that multiplied with the square of the ''effective'' neutrally stable 10-m wind provides estimates of the surface wind stress.

An evaluation of the accuracy of this in situ model was conducted in October 1995, during the first phase of the SWADE experiment. At discus buoy ''North,'' a K-Gill anemometer was measuring u_* continuously, with outputs available at hourly intervals for comparison with the WAM-derived u_*. Over a continuous 2.5-day interval the magnitudes of u_* ranged from 0.05 to 0.6 m s^{-1}. The two different estimates of u_* were usually in good agreement. The mean difference between the two was 0.04 m s^{-1}, and the rms difference for this interval was 0.08 m s^{-1}.

4. K_u-band model function studies

Since the K_u-band model function for friction velocity was developed using the FASINEX data with empirical techniques, it is important to conduct independent tests and evaluations of this model. Each daily dataset was collected over flight intervals of approximately 4 h or longer. The normalized radar cross-sectional measurements were converted into friction velocity estimates at specific locations and times using this model. These u_* estimates were then compared with the in situ estimates discussed above. They were updated every hour and spanned the entire SWADE region of interest.

A latitude and longitude grid with 0.25° resolution of friction velocity estimates was developed from the OWI–Miami dataset and technique. The area over which these friction velocity estimates are made spans the same regions of the ocean over which the aircraft scatterometer operated. The friction velocity maps are among the several variables (such as significant wave height, mean frequency, neutral stability wind, drag coefficient, and wind direction), that were produced. Examples of this dataset for 7 March 1991 are shown in Figs. 1–3. Averages of four sequential hourly grids of the neutral stability wind speed, drag coefficient, and friction velocity are shown in these figures. The 0.25° separations between adjacent values were interpolated to produce a finer spatial mesh. The strong spatial variability of the drag coefficient as seen in Fig. 2 is a clear message that the neutral stability winds are not a sufficient indicator of the momentum flux at the air–sea interface.

The estimates of friction velocity inferred from the K_u-band scatterometer (A_0 data) must be interpreted as spatial and temporal averages of 15 km and 2 min, respectively. An example of these results is presented from the 7 March dataset in Fig. 4. There are 19 useful flight paths on this day. A vertical line and a filled circle whose height is scaled to the u_* magnitude is placed at the individual average location of each path center. These locations are the approximate center of the flight path for that average NRCS measurement. An interpolation program was used to create a mesh surface that estimates the u_* throughout the observed region from these 19 points. Because of the intense spatial variability of u_*, this mesh surface obscures the view of some of the individual points. It should be kept in mind that this dataset was collected over a time interval that extends to 4 h, so that true simultaneity among all these points is not possible. The strong spatial variations apparent in this figure are seen to have much in common with the u_* plot from the OWI–Miami estimates. These gradients occur in the radar data because the flight path locations were intentionally selected to cross the western edge of the Gulf Stream. The strong sea surface temperature variations in this region can be seen in the Advanced Very High Resolution Radiometer (AVHRR) thermal infrared color imagery displayed by Caruso et al. (1994b, see their appendix E).

Because of the appreciable time differences among the radar estimates, a more meaningful comparison was to match each acquisition time of the radar data with one of the times at which the OWI–Miami u_* maps were created (e.g., Fig. 3). Each aircraft estimate of u_* can be compared with the closest u_* value (within 0.1° latitude and longitude, and within a 0.5-h interval) from

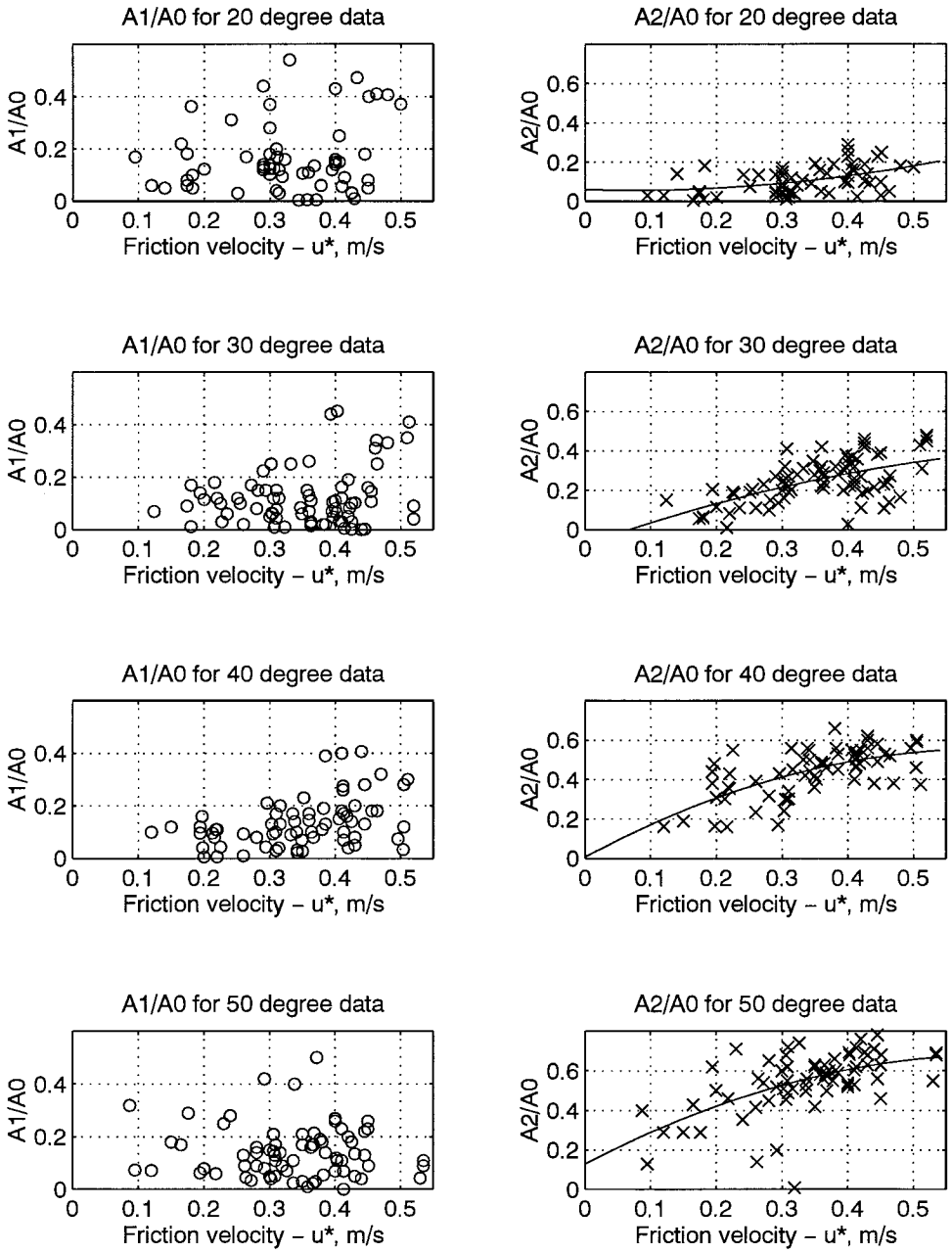

FIG. 11. The corresponding C-band Fourier series terms, A_1 and A_2, that accompany each data point in Fig. 10, normalized by A_0, versus u_*. Separate plots for each incidence angle. Note the general increase in the magnitude of A_2/A_0 with incidence angle and with u_*. The solid curves plotted in each A_2/A_0 graph represent a second-order polynomial fit to these data. See Table 1 for coefficients and R.

this in situ model. The closer these values agree, the stronger the support for the validity of the FASINEX algorithm. However, it should be kept in mind that the in situ estimates of u_* are also subject to some degree of error because of physical processes, the spatial resolution of the fundamental data upon which it is based, and a possible time difference of 30 min.

Data from 8 days within this period were combined into a plot of scatterometer derived u_* versus that produced by OWI–Miami. The comparison between the two different u_* estimates can be seen in Fig. 5a. Two of the days in which radar data were collected could not be analyzed because of either unreliability or unavailability of some data. The agreement is good. The regression line and correlation coefficient are also presented. These data were grouped into abscissa bins (0.025 m s^{-1} wide); the mean of the ordinate and its standard deviation are shown in Fig. 5b.

A possible cause of error may be the inability of this in situ model to produce a reliable estimate of the drag coefficient and friction velocity when the sea spectrum is a strong mixture of both wind-driven seas and incoming swell, and whose propagating directions are at large oblique angles. This condition existed on 28 February and 6 March. On 28 February, the sequence of flight paths took place in the proximity of three different buoys, which were widely separated by about 100 km. The relevant buoy locations for this day's flight are shown on a map in Fig. 6, along with the flight tracks drawn with solid line segments. Buoys labeled C, E, and CERC served as destination points for the aircraft and critical data sources for the in situ analysis described above. At the time of radar observations the directional wave spectra at each of these buoys show a combination of both wind-driven seas (from the southwest) and westerly swell (Caruso et al. 1994b). The directional spectra are presented using polar wavenumber diagrams with contours to represent magnitudes and are overlaid in this map near the respective buoys. Each polar spectrum is labeled with the time of data collection; the wind speed direction (meteorological convention); the mean wave direction, ''md'' (oceanographic convention); and the direction of the spectral peak, ''pd.'' A sample of the one-dimensional frequency spectrum for the CERC wave data is shown near the bottom of this map, next to the CERC directional spectra. It is obvious that on 28 February, at the time of the radar measurement the wave spectrum displayed strong bimodal properties. This complicated spectrum structure cannot be accurately included in the drag coefficient derivation. Any error in this estimated drag coefficient will induce an error in the u_* estimate. A similar situation existed for the wave spectrum on 6 March.

A quantitative assessment of this phenomenon is seen in Fig. 7, in which we examine each day's results separately. The comparison between the u_* estimates from the scatterometer and that of the in situ analysis are plotted for each of the 8 days. Both 28 February and 6 March are different in that a majority of observations have the property that the two u_* estimates differ by more than 25%. The other 6 days show a more consistent agreement between the scatterometer and in situ estimates of u_*. When the data from these 6 days are all combined in a composite single plot (now without the 28 February and 6 March data) in Fig. 8a, the effective agreement is clearly seen to improve. The multiple correlation coefficient R is now 0.83, compared with $R = 0.72$ for the unmodifed dataset. The slope of the regression line, m, is now equal to 1.01 in Fig. 8a compared with $m = 0.83$ in Fig. 5a. The binned data of Fig. 8b also shows a reduced standard deviation in most of the bins. Another possible source of error may be the rapid spatial variability of u_* in some locations with steep drops in magnitude, and the limited ability of the meteorological model to precisely position and resolve these sharp spatial changes in these relatively small regions because of its larger spatial resolution.

Wind direction estimates were also compared. The azimuth scan measurement of the radar cross section by the scatterometer is acquired over a span of about 15 km across a flight track (Nghiem et al. 1995). Past experience with scatterometer studies indicates the azimuthal maximum is usually observed looking upwind. Using this indicator on each scatterometer circular scan, the wind direction was estimated and then compared with the wind direction estimates by the OWI–Miami group. This comparison can be seen in Fig. 9 for 7 days of data for all incidence angles: 20°, 30°, 40°, and 50°, plotted separately. Numerous errors can be seen, mostly those due to a 180° ambiguity caused by an inversion of the NRCS maximum; it occurs when looking downwind instead of upwind. This is more prevalent at the 20° and 30° incidence angles than at 40° and 50°. While some allowance should be made for surface variability across the 10-km flight path crossed during one-half the antenna rotation, the preponderance of this evidence is clear. The 40° and 50° incidence angles have the fewest errors because at these incidence angles, the ratio of the NRCS maximum looking upwind to downwind is generally higher. This has important implications for the NSCAT model function, in that the ability to estimate wind speed and direction depends on having a sufficiently larger upwind to downwind ratio. In most cases, no significant differences in the errors due to the polarization of the electromagnetic wave (vertical versus horizontal) were observed.

5. C-band model for friction velocity

This model has the same general structure (a three-term Fourier cosine series) as the well-known K_u-band function (Wentz et al. 1984). The data used in this development were obtained from 9 of the 10 scatterometer flights. The experiment days of 28 February and 1, 2, and 4–9 March were analyzed. C-band NRCS data are available at incidence angles from 20° to 50° in 10° steps, and it has been processed to calculate the three Fourier coefficients (A_0, A_1, A_2). The coefficients A_0, A_1/A_0, and A_2/A_0 were plotted versus u_*, which was obtained from the simultaneous K_u-band data used with the FASINEX algorithm.

The friction velocity u_* is estimated from the K_u-band A_0 measurement made over the same or a closely adjacent flight segment. The incidence angle of the K_u-band radar is selected independently of the C-band radar incidence angle. The only requirement is that it be at an angle at which there is an existing K_u-band algorithm between A_0 and u_*; these are at 20°, 30°, 40°, and 50° (Weissman et al. 1994).

The results shown in Fig. 10 show the dependence of the C-band A_0 term on friction velocity. The four different incidence angles produce four distinguishable datasets that separate clearly in magnitude and in their

TABLE 1. Coefficients for second-order polynomial for A_2/A_0, u_* variable (see Fig. 11).

Incidence angle θ_i	Polynomial coefficients m_1	m_2	m_3	Correl. coeff. R
20°	0.059	−0.0905	0.671	0.44
30°	−0.756	1.172	−0.680	0.59
40°	0.008	1.78	−1.445	0.66
50°	0.13	1.73	−1.354	0.58

dependence on friction velocity. The linear regression lines that were fit to each of the incidence angles' data have slopes that represent the exponent of a power-law fit of A_0 to u_* at each angle. This slope gradually increases with the incidence angle: from 0.72 at 20° to 1.53 at 50°. These exponent magnitudes are all smaller than the values found for the K_u-band model function during FASINEX (Weissman et al. 1994). Generally speaking, this is in qualitative agreement with the wind speed model function being developed for the *ERS-1* C-band scatterometer (Bentamy et al. 1994).

The principle underlying these regression analyses is that the abscissa is much less susceptible to errors than the ordinate. A more general regression analysis allows the possibility for both quantities to contain random errors. A separate reanalysis, using a technique presented in Draper and Smith (1981), gives slightly different regression coefficients. However, these differences do not produce significant deviations from the results presented in Fig. 10.

The two other Fourier series coefficients, A_1 and A_2, are observed here to have very different and distinctive properties in Fig. 11. The A_1/A_0 normalized term shows generally small and highly random values at all the incidence angles. It appears to be too small (the average seems to be about 0.1) to have a critical role in the C-band scatterometer algorithm. The A_2/A_0 terms also shown in Fig. 11 affect the upwind/crosswind ratio and have an appreciable magnitude that increases with u_* and with incidence angle. We see an increase in A_2/A_0 of a factor of approximately 5 between 20° and 50° incidence angles. However, the dependence of A_2/A_0 on friction velocity is seen to have interesting properties once u_* reaches 0.4 m s^{-1}. For θ_i (incidence angle) = 30°, A_2/A_0 appears to decrease with $u_* \geq 0.4$ m s^{-1}; but for $\theta = 40°$ and 50°, A_2/A_0 seems to level off for u_* up to 0.5.

Second-order polynomials in u_* were fit to each of these A_2/A_0 datasets in Fig. 11 and are plotted in each graph as solid lines. The parameters of each of these polynomials is listed in Table 1, and each is accompanied by the multiple correlation coefficient R for that collection of values.

In order to use this A_0 function in the analysis of satellite or aircraft data where the incidence angle can lie anywhere between 20° and 50°, the resolution of the functional dependence on incidence angle was improved using linear interpolation between these decadel angles.

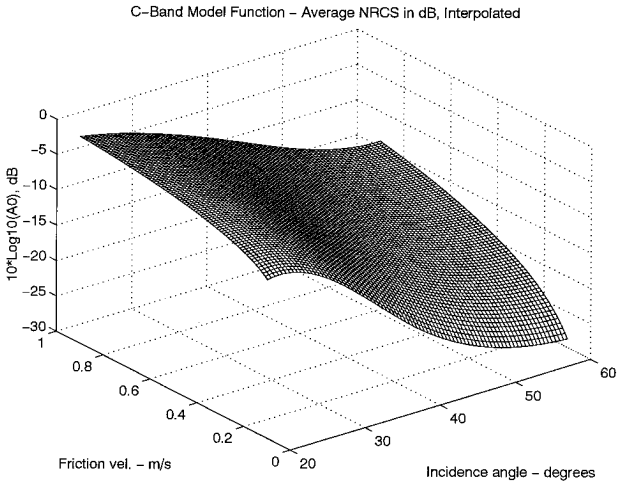

FIG. 12. The graphical representation of the A_0 term, in decibels, a function of both friction velocity and incidence angle, for the C-band model function. It is computed using an interpolation between the power-law regression lines fit to the data of Fig. 10, to extend the results to incidence angles between the measured cases of 20°, 30°, 40°, and 50°.

The resulting A_0 is plotted as a function of the two independent variables, in Fig. 12. This A_0 function can be used with the *ERS-1* NRCS data to infer the magnitude of u_*. Preliminary studies using this interpolated function have produced excellent results (Davidson et al. 1995; Weissman 1995).

6. Summary

The next logical step in evaluating the FASINEX K_u-band model function has been performed. The friction velocity estimates derived from the NRCS measurements were compared with the best available spatial and temporally coincident data on a scale that had not been previously possible. In every comparison dataset, the issue of the accuracy of the primary ''standard'' measurement must be clearly understood and explained. Generally speaking, in oceanographic experiments the most accurate physical measurements are associated with calibrated meteorological and oceanographic instruments on buoys, ships, stationary oceanographic towers, or low-flying aircraft. With respect to the type of resolution each of these could have, only the aircraft platform is restricted in terms of the time duration; the other platforms permit continuous monitoring of the desired quantities indefinitely. But, with respect to spatial resolution, the price of this high accuracy is to limit the measurements to a single point in space. During SWADE there were no low-flying aircraft that were measuring the air–sea fluxes. Therefore there is no available technique that extends the same accuracy of ''point'' instruments to the large spatial areas traveled and observed by the scatterometer, in a sufficiently short time. The surface conditions—winds, waves, and momentum flux—provided by the OWI techniques are the best compromise dataset that is available with which to compare the scat-

terometer results. They represent a major innovation in estimating conditions at the air–sea interface over a wide area. However, future extension of these studies is clearly indicated, to continue the development of this technique. Some of the assumptions used in this analysis should be critically reexamined. For example, the implications of neglecting the finite ocean depth in applying the WAM-4 model should be considered. Also the possible wave–current interaction was not accounted for in these calculations, but it could be reconsidered in a future experiment in which detailed current data would be available. Another quantity that is of interest is the spatial variation of the air–sea temperature difference and the atmospheric stratification, with sufficiently high spatial resolution.

By choosing the 6 days during SWADE within which the combined meteorological and sea conditions were least complicated, we were able to achieve excellent agreement between the two different friction velocity estimates. It is expected that this FASINEX K_u-band model function will be applied to the satellite-based NSCAT measurements when they become available. These will provide estimates of the friction velocity at the sea surface on a global scale. However, the evaluation of its accuracy on this global scale becomes a more tenuous process than what was done here with the SWADE data, due to the lack of surface instruments that can match the space and time scales of the satellite scatterometer swath. The evaluation of the satellite measurements and model function will require the observation of the regional, basin, and global-scale predictions (both meteorological and oceanographic) that are created from its data analysis. For oceanographic processes these will require long-duration datasets (months and years). For meteorological studies and predictions, a rapid analysis using single satellite passes is usually the preferred situation.

The use of the difference between the upwind and downwind maximum in the azimuthal scan of the normalized radar cross section (NRCS) is the usual method by which the wind direction is estimated. Previous results with K_u-band model function studies have found that the magnitude of the NRCS looking upwind is larger than that looking downwind, *on the average* (Wentz et al. 1984; Weissman et al. 1994). This is equivalent to the A1 term in the Fourier series model being a positive number. However, this difference decreases with incidence angle and can display random fluctuations (and sign reversal) in response to the wide variety of effects induced by nonequilibrium seas. The results shown in Fig. 9, where the radar-derived estimates of wind direction are compared with the in situ data, indicate some departure from the expectations for the 20° and 30° SWADE data. At these angles, there is a higher probability (about 50% for 20°, and about 35% for 30°) that a radar-derived estimate of direction will be in error by 180°, because of the frequently observed inversion (negative A1). Results are much improved for the 40° and 50° observations, where the direction estimates are correct about 85% of the time.

The findings described above for the 20° analysis are not significantly different from what was determined in the data analysis of the FASINEX experiment. The FASINEX findings for A_1/A_0 at this angle for V-pol and H-pol are that it is ''small, highly variable, and almost negligible and that at 20° it is effectively zero'' (Weissman et al. 1994). The results for the 30° data in Fig. 9 also display an appreciable number of errors in the directional estimation. These also agree with the FASINEX 30° results in which the A_1/A_0 estimates tended to be lower (on average) than the higher incidence angles and where negative values were seen to occur. It can therefore be concluded that the results presented in Fig. 9 are in substantial agreement with the K_u-band analysis conducted with the FASINEX data.

The new results for a C-band model function for friction velocity are believed to be the first attempt to develop this type of algorithm using measured data. It also begins an era in which a K_u-band scatterometer is used to produce ''in situ'' estimates of the surface friction velocity. The justification for this application is the successful comparison between the u_* inferred from the K_u-band scatterometer and that produced from the in situ analysis by the OWI group, as presented in section 4.

The properties of the A_0 versus u_* power-law approximations for each incidence angle shown in Fig. 10 are reasonable in the sense that the magnitude of the exponent increases with incidence angle from 20° to 50° and that they are smaller than the corresponding K_u-band V-pol cases. The next phase of evaluating this algorithm was to apply it to the data collected by the *ERS-1* C-band satellite scatterometer in conjunction with supporting surface measurements. An opportunity arose to utilize this algorithm with *ERS-1* passes near the coast of Norway during the Norwegian Continental Self Experiment 1991 Calibration/Validation Experiment for the newly launched instrument. In situ measurements, including the friction velocity, were provided by ship-based meteorological instruments (Davidson et al. 1995). Passes were analyzed whereby this C-band algorithm for A_0, shown in Fig. 12, was used to estimate the magnitude of u_*. These were then compared with the coincident shipboard measurements. The results show very good agreement across the range of u_* from 0.1 to 1 m s^{-1}, with differences sometimes less than 10%.

Acknowledgments. This research was sponsored by the Physical Oceanography Program of the National Aeronautics and Space Administration, Washington, D.C. The research performed by D. Weissman was sponsored through Grant NAGW-468 with Hofstra University. The research performed by R. McIntosh, S. Carson, and J. Carswell was supported through a contract with the Microwave Remote Sensing Laboratory of the University of Massachusetts. The research performed by F. Li, S. Lou, S. Nghiem, and G. Neumann was performed at the Jet Propulsion Laboratory, California Institute of Technology,

under contract with NASA. The work of H. Graber was sponsored by the Office of Naval Research.

REFERENCES

Anderson, R. J., 1993: A study of wind stress and heat flux over the open ocean by the intertial-dissipation method. *J. Phys. Oceanogr.*, **23,** 2153–2161.

Barnier, B., M. Boukthur, and J. Verron, 1991: Use of satellite scatterometer winds to force an ocean general circulation model. *J. Geophys. Res.*, **96** (C12), 22 025–22 042.

——, J. Capella, and J. J. O'Brien, 1994: The use of satellite scatterometer winds to drive a primitive equation model of the Indian Ocean: The impact of bandlike sampling. *J. Geophys. Res.*, **99** (C7), 14 187–14 196.

Bentamy, A., Y. Quilfen, P. Queffeulou, and A. Cavanie, 1994: Calibration of the ERS-1 Scatterometer C-band model. IFREMER/Brest Tech. Rep. DRO/OS-94-01, 72 pp. [Available from IFREMER, Brest, BP 70 29280, Plouzane, France.]

Cardone, V. J., H. Graber, R. Jensen, S. Hasselmann, and M. Caruso, 1995: In search of the true surface wind field in SWADE IOP-1: Ocean wave modeling perspective. *The Global Atmosphere and Ocean System*, Vol. 3 (2–3), Gordon and Breach Science, 107–150.

Carson, S., R. McIntosh, A. Paylor, F. Li, G. Neumann, and D. McLaughlin, 1992: C-Band measurement of radar backscatter from the ocean surface during SWADE. *IGARSS '92 Proc. Vol. I, IEEE Geoscience and Remote Sensing Symp.*, Vol. 1, Houston, TX, IEEE, 693–695.

Carswell, J. R., S. Carson, R. McIntosh, F. Li, G. Neumann, D. McLaughlin, J. Wilkerson, P. Black, and S. Nghiem, 1994: Airborne scatterometers: Investigating ocean backscatter under low and high wind conditions. *Proc. IEEE*, **82** (12), 1835–1860.

Caruso, M. J., H. C. Graber, R. E. Jensen, and M. A. Donelan, 1994a: Surface wave dynamics experiment. U.S. Army Corps of Engineers Tech. Rep. CERC-93-6, Rep. 2, 294 pp.

——, K. A. Kelly, J. Metzger, and H. Hurlburt, 1994b: Comparison of ERS-1 scatterometer and ECMWF wind forcing in the Kuroshio extension region. *American Geophysical Union Fall Meeting*, San Francisco, CA, Amer. Geophys. Union.

Cavaleri, L., L. Bertotti, and P. A. E. M. Janssen, 1994: Wave-dependent drag coefficient. *Dynamics and Modelling of Ocean Waves*, G. J. Komen, L. Cavaleri, M. Donelan, K. Hasselmann, S. Hasselmann, and P. A. E. M. Janssen, Eds., Cambridge University Press, 316–319.

Davidson, K. L., D. E. Weissman, E. van Halsema, and R. Onstott, 1995: Coastal applications of scatterometer wind algorithms. *OCEANS '95 Conf. Proc.* San Diego, CA, IEEE, 1251–1258.

Donelan, M., F. Dobson, S. Smith, and R. Anderson, 1993: Dependence of sea surface roughness on wave development. *J. Phys. Oceanogr.*, **23,** 2143–2149.

Freilich, M. H., 1985: Science opportunities using the NASA Scatterometer on N-ROSS. NASA Jet Propulsion Laboratory Pub. 84–57, 42 pp.

——, 1995: Surface wind data from ERS-1 measurements. 1995 U.S. World Ocean Circulation Experiment Rep., Implementation Rep. 7, 56 pp. [Available from Dept. of Oceanography, Texas A&M University, College Station, TX 77843-3146.]

——, and R. S. Dunbar, 1993: A preliminary C-band scatterometer model function for the ERS-1 AMI instrument. *First ERS-1 Symp.*, Cannes, France, European Space Agency, 1–4.

Graber, H. C., V. Cardone, R. Jensen, S. Hasselmann, H. L. Tolman, and L. Cavaleri, 1994: The accuracy of wind field description. *Dynamics and Modelling of Ocean Waves*, G. J. Komen et al., Eds., Cambridge University Press, 285–293.

——, R. E. Jensen, and V. J. Cardone, 1995: Sensitivity of wave model predictions on spatial and temporal resolution of the wind field. *Proc. 4th Int. Workshop Wave Hindcasting and Forecasting.* Banff, AB, Canada.

Geernaert, G. L., 1990: Bulk parameterizations for the wind stress and heat fluxes. *Surface Waves and Fluxes*, Vol. I, *Current Theory*, G. L. Geernaert and W. L. Plant, Eds., Kluwer Academic, 91–172.

Jahne, B., and K. S. Riemer, 1990: Two-dimensional wave number spectra of small-scale water surface waves. *J. Geophys. Res.*, **95** (C7), 11 531–11 546.

Janssen, P. A. E. M., 1991: Quasi-linear theory for wind-wave generation applied to wave forecasting. *J. Phys. Oceanogr.*, **21,** 1631–1642.

——, 1992: Experimental evidence of the effect of surface waves on the airflow. *J. Phys. Oceanogr.*, **22,** 1600–1604.

Komen, G. J., 1994: Boundary conditions and wind profile over waves. *Dynamics and Modelling of Ocean Waves*, G. J. Komen et al., Eds., Cambridge University Press, 53–57.

Legler, D. M., and J. J. O'Brien, 1993: Comparison of ERS-1 scatterometer and Florida State University tropical winds. *Proc. Second ERS-1 Symp.*, Hamburg, Germany, European Space Agency, 1–4.

Li, F., W. Large, W. Shaw, E. J. Walsh, and K. Davidson, 1989: Ocean radar backscatter relationship with near-surface winds: A case study during FASINEX. *J. Phys. Oceanogr.*, **19,** 342–353.

McLaughlin, D. J., R. E. McIntosh, A. Pazmany, L. Hevizi, and E. Boltniew, 1991: A C-band scatterometer for remote sensing the air–sea interface. *IEEE Trans. Geosci. Remote Sens.*, **29** (2), 260–267.

Nghiem, S. V., F. Li, S. Lou, G. Neumann, R. McIntosh, S. Carson, J. Carswell, E. Walsh, M. Donelan, and W. Drennen, 1995: Observations of radar backscatter at K_u and C bands in the presence of large waves during SWADE. *IEEE Trans. Geosci. Remote Sens.*, **33** (3), 708–725.

Nordeng, T. E., 1991: On the wave age dependent drag coefficient and roughness length at sea. *J. Geophys. Res.*, **96** (C4), 7167–7174.

O'Brien, J. J., 1982: Scientific opportunities using satellite surface wind stress measurements over the ocean. Rep. of the Satellite Surface Stress Working Group, 143 pp.

Phillips, O. M., 1988: Radar returns from the sea surface—Bragg scattering and breaking waves. *J. Phys. Oceanogr.*, **18,** 1065–1074.

Pierson, W. J., Jr., 1990: Dependence of radar backscatter on environmental parameters. *Surface Waves and Fluxes*, Vol. II, *Remote Sensing*, G. L. Geernaert and W. L. Plant, Eds., Kluwer Academic, 173–220.

Plant, W. J., 1990: Bragg scattering of electromagnetic waves from the air/sea interface. *Surface Waves and Fluxes*, Vol. II, *Remote Sensing*, G. L. Geernaert and W. L. Plant, Eds., Kluwer Academic.

Smith, S. D., 1988: Coefficients for sea surface wind stress, heat flux, and wind profiles as a function of wind speed and temperature. *J. Geophys. Res.*, **93,** 15 467–15 472.

——, and Coauthors, 1992: Sea surface wind stress and drag coefficients: The HEXOS results. *Bound.-Layer Meteor.*, **60,** 109–142.

Stage, S. A., and R. A. Weller, 1985: The Frontal Air–Sea Interaction Experiment (FASINEX): Part I: Backround and Scientific Objectives. *Bull. Amer. Meteor. Soc.*, **66,** 1511–1520.

——, and ——, 1986: The Frontal Air–Sea Interaction Experiment (FASINEX). Part II: Experiment plan. *Bull. Amer. Meteor. Soc.*, **67,** 16–20.

Weissman, D. E., 1994: Studies of a C-band model function for friction velocity using coincident, simultaneous Ku-band scatterometer measurements. *OCEANS '94 Conf. Proc.*, Brest, France, IEEE.

——, 1995: Scatterometer measurements of ocean surface stress from aircraft and from ERS-1. *OCEANS '95 Conf. Proc.*, San Diego, CA, IEEE.

——, K. Davidson, R. Brown, C. Friehe, and F. Li, 1994: The relationship between the microwave radar cross section and both wind speed and stress: Model function studies using Frontal Air–Sea Interaction Experiment data. *J. Geophys. Res.*, **99** (C5), 10 087–10 108.

Weller, R. A., M. A. Donelan, M. G. Briscoe, and N. E. Huang, 1991: Riding the crest: A tale of two wave experiments. *Bull. Amer. Meteor. Soc.*, **72,** 163–183.

Wentz, F. J., S. Peterherych, and L. A. Thomas, 1984: A model function for ocean radar cross section at 14.6 GHz. *J. Geophys. Res.*, **89,** 3689–3704.